Effect of Canyons and Their Interaction on Ground Response to Vertically Traveling SH Waves

A. Eslami H.[1], S.A. Anvar[2], M. Jahanandish[3], and A. Ghahramani[4]

1. Ph.D. Candidate, Dept. of Civil & Environmental Engineering, Shiraz University Shiraz, I.R. Iran, email: eslami@shirazu.ac.ir
2. Assistant Professor, Dept. of Civil & Environmental Engineering, Shiraz University, Shiraz, I.R. Iran
3. Associate Professor, Dept. of Civil & Environmental Engineering, Shiraz University, Shiraz, I.R. Iran
4. Professor, Dept. of Civil & Environmental Engineering, Shiraz University, Shiraz, I.R. Iran

ABSTRACT

In this paper the dynamic response of the ground surface subjected to vertically traveling two dimensional harmonic SH waves in the presence of a single or two canyons is investigated using boundary element method. The models consist of one and two semicircular canyons cut from a homogeneous, linear and viscoelastic half space. The total response is computed by summing up the responses of free field and scattered waves. The former is calculated from the closed form solution of propagated waves in the half space and the latter from the boundary element method. For this, surface irregularities are discretized by linear elements and influence coefficient matrices are obtained by using harmonic fundamental solutions. To validate the technique, the response of a single canyon and its nearby ground surface due to harmonic SH waves with different frequencies is determined and compared with the existing closed form solution. Then, the response of double canyon is determined by the same procedure. Results of analyses indicate that the distance between canyons is a key parameter that affects the surface displacement amplitude of both canyons. It is demonstrated that when this distance is increased, the response of both canyons approach to that of a single one. Furthermore, it is shown that the interaction is also very much dependent on the frequency of the incident wave.

Keywords:
Boundary element;
Wave propagation;
Viscoelastic material;
Single canyon;
Double canyon;
SH wave

1. Introduction

The effect of surface topography on amplification of incident seismic waves has been the subject of extensive researches in the past forty years. The seismic waves are diffracted by the surface irregularities like hills and canyons. To investigate this phenomenon, different methods have been suggested which can generally be classified into analytical and numerical approaches. Free field solution of *P*, *SV* and *SH* waves can be obtained analytically by superposing incident and reflected waves in a half space. There are closed form solution for wedge-shaped elastic medium [1] as well as *V*-shaped canyons [2] and triangular hills [3] subjected to incident *SH* waves. Closed form solutions for two dimensional semicircular [4] and semielliptical [5] canyons have also been obtained by eigenfunction expansion method [6]. Analytical solutions are also available for two dimensional semicircular [7] and circular-arc cross-section hills [8] on elastic half space subjected to harmonic *SH* waves. In order to achieve more consistent results in higher frequencies, different analytical approach has been developed by Lee et al [9]. The limitation of the closed form solutions is that their applications are almost restricted to two dimensional simple surface topographies. Therefore, numerical methods are required to calculate the dynamic response of topographies of more complicated forms. In Aki-Larner method [10], the scattered wave field is expressed in terms of discrete wave number. This method was then extended to scattering of *P*, *SV* and *SH* waves in time domain [11]. The method has been developed to consider arbitrary surface topography and subsurface layering only for incidence of *SH* waves [12].

Domain methods such as finite element and finite

difference methods have also been applied to study the scattering problems. Diffraction of *SH* waves was performed by finite difference method [13]. Finite element method is one of the most powerful numerical methods in almost all geotechnical fields as well as the wave scattering problem. However, in such domain methods the fictitious boundaries, considered for limiting the medium extent, reflect back the outgoing waves into the medium. In other words, the radiation condition is not satisfied. To remove this deficiency, some techniques have been proposed. It is evident that if the surrounding fictitious boundaries are adopted far away from the irregularity, its effects would decrease. But, analysis of larger models require more computational time. Other techniques such as infinite elements [14] and absorbing boundaries [15] have been used in diffraction of *SH* waves by Zhang and Zhao [16] and Liu and Lu [17], respectively.

Boundary element method (*BEM*) is a numerical method in which the radiation condition is satisfied automatically. The method has been widely used in dynamic analysis of homogeneous media and also in scattering of *SH* waves, [18]. Semi-cylindrical [19], and non-axisymmetric, [20], canyons subjected to *P*, *SV* and *SH* waves have been analyzed by this method. This method has been successfully applied to two dimensional [21] and three dimensional [22] ground response analyses. *BEM* has also been combined with other methods and the resulting hybrid techniques have been effectively used. In discrete wave number boundary element method, the direct boundary element method is combined with green functions of discrete wave number. This hybrid method has been applied to diffraction of *P*, *SV* and *SH* waves in two [23], and three [24], dimensional domains.

The studies of Geli et al [12], and Bard and Tucker [25], showed that the observed amplification measured in the field is greater than what is predicted by numerical simulation. Sanchez-Sesma and Campillo [26], showed that a relatively simple irregularity may result in significant variations in and around the irregularity. However, more precise modeling results in more accurate results. Soil layering and surface irregularities in three dimensions increase the complexity of the problem of the scattering of the waves. The effect of multilayered soil with irregular interface on the scattering of *SH* waves has been considered by Ding and Dravinski, [27]. The interaction of adjacent irregularities may also cause the response of ground motion to differ from the response of individual irregularities.

The effects of canyon and interaction of adjacent semicircular canyons on the diffraction of harmonic *SH* waves is investigated in this paper. It is demonstrated that the frequency of incident waves and the distance between canyons can considerably affect the results.

2. The BE Formulation

The *BE* method is a powerful numerical technique for the analysis of homogeneous elastic medium in the static and dynamic states. Neglecting the body forces, the governing boundary integral equation for a two dimensional homogeneous, elastic and isotropic medium can be obtained by using Betti's reciprocal theorem as follows:

$$c(\xi)u(\xi) = -\int_L p_z^*(\xi,\chi)u(\chi)dL(\chi) + \int_L p(\chi)u_z^*(\xi,\chi)dL(\chi) \quad (1)$$

where ξ denotes the source point and χ the observation point along the boundaries, u and p are displacements and tractions of points on the boundary, respectively, dL is the incremental length along the boundary navigated counterclockwise, c is the jump term which is equal to 0.5 for smooth boundaries, and $u_z^*(\xi,\chi)$ and $p_z^*(\xi,\chi)$ are time-harmonic fundamental solutions representing displacement and traction at the observation point χ, due to a unit harmonic point load applied at the source point ξ in an infinite region. Fundamental solutions for two dimensional time-harmonic anti-plane problems are as follows [28]:

$$\begin{cases} u_z^* = \dfrac{1}{2\pi\mu} K_0\left(\dfrac{i\omega r}{C_s}\right) \\ p_z^* = \dfrac{1}{2\pi}\dfrac{i\omega}{C_s}\dfrac{\partial r}{\partial n} K_1\left(\dfrac{i\omega r}{C_s}\right) \end{cases} \quad (2)$$

where μ is the shear modulus, K_0 and K_1 are the modified Bessel functions of second kind and order zero and one, respectively, r is the distance between the source and the observation points, and ω and C_s

are the frequency and propagation velocity of *SH* wave, respectively. C_s can be written as:

$$C_s = \sqrt{\frac{\mu}{\rho}} \tag{3}$$

where ρ is the mass density of the material.

The boundary integral equation can be determined by discretization of the boundary into elements by proper selection of nodes. Here, isoparametric two-noded linear element is adopted. The convoluted form of Eq. (1) is then written for every boundary points as follows [28]:

$$c_q u_q + \sum_{e=1}^{nElems}\left[\int_{L_e} p_z^*\{N\}^T dL_e\{u^e\}\right] = \sum_{e=1}^{nElems}\left[\int_{L_e} u_z^*\{N\}^T dL_e\{p^e\}\right] \tag{4}$$

where q is the node number and it also corresponds to q^{th} degree of freedom. The column vectors $\{u^e\}$ and $\{p^e\}$, represent the nodal displacement and traction vectors, respectively, and $\{N\}$ is the interpolation vector, *nElems* is the number of linear boundary elements and L_e is the length of the e^{th} element. c_q is the jump term of node number q which is equal to 0.5 for smooth boundaries, as mentioned before. For corner nodes, the value of c_q can be computed as:

$$c_q = \frac{\alpha}{2\pi} \tag{5}$$

where α is the internal angle of the corner in radians. The integral over each element is carried out in the local coordinate system using standard Gauss quadrature technique. Successive application of Eq. (4) to points at the boundary results in a system of linear algebraic equations of the following form [29]:

$$[F]\{u\} = [G]\{p\} \tag{6}$$

where $[F]$ and $[G]$ are the influence coefficients matrices and the vectors $\{u\}$ and $\{p\}$ contain the nodal displacements and tractions of all boundary nodes, respectively. After rearranging the known and unknown displacements and tractions in Eq. (6), the resulted matrix equation can be easily solved for unknown displacements and tractions at the boundary.

3. Singular Integrals for Linear Boundary Elements in Anti-Plane Problems

When the source point coincides with the observation point, the distance *r* between the two becomes zero and singularities appear in both right and left hand sides of Eq. (4). The elements in which the singularity occurs are called singular elements.

3.1. Weak Singularities

The right hand side of Eq. (4) has two weak singular integrals depending on whether the source point coincides with the beginning or the end nodal point of the singular linear element. These singularities can be handled by means of analytical integration as described, hereafter.

Case 1: In this case the source point coincides with point **a**; the beginning node of the element, see Figure (1). All integrals over each singular or non-singular element are carried out in the local coordinate system in which *s*, the local coordinate parameter, varies between -1 and +1.

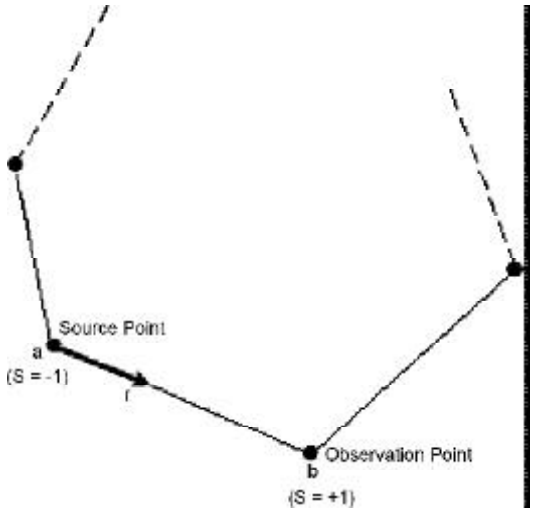

Figure 1. Position of source and observation points in case 1 singularity.

The position of observation point varies between points **a** and **b**. In Figure (1) the observation point is located at the end of the singular element, point **b**. As the observation point approaches the source point, *r* goes to zero and *s* = -1 and singularity occurs in the *R.H.S.* integral of Eq. (4), which takes the following form upon substitution of Eq. (2).

$$\int_s \{N\}^T \frac{1}{2\pi\mu} K_0\left(\frac{i\omega r}{C_s}\right) J\, ds \tag{7}$$

where

$$r = \left(\frac{1+s}{2}\right) L_e \tag{8}$$

In Eq. (7), J is the Jacobian of the transformation. Considering the following equations [30]:

$$\lim_{z\to 0} K_0(z) = -ln(z) \tag{9}$$

and

$$K_0\left(\frac{i\omega r}{C_s}\right) = K_0\left(\frac{i\omega r}{C_s}\right) + ln\left(\frac{1+s}{2}\right) - ln\left(\frac{1+s}{2}\right) \tag{10}$$

the integral in Eq. (7) can be written as:

$$\int_s \{N\}^T \frac{1}{2\pi\mu}\left[K_0\left(\frac{i\omega r}{C_s}\right) + ln\left(\frac{1+s}{2}\right)\right] J\, ds - \int_s \{N\}^T \frac{1}{2\pi\mu} ln\left(\frac{1+s}{2}\right) J\, ds \tag{11}$$

The first integral in Eq. (11) is not singular at s = -1 and so the standard Gauss quadrature technique can be applied to numerically evaluate it. The second integral of Eq. (11) is still singular but because of its logarithmic form can be numerically evaluated using the logarithmic Gauss quadrature formulation [29].

Case 2: Figure (2) shows the situation in which the source point coincides with point **b** at the end of singular element and the observation point is located at point **a**. When observation point coincides with the source point singularity occurs which corresponds to s = +1. The singularity in this case can be handled exactly the same as in case 1 except for the term $ln\left(\frac{1+s}{2}\right)$ which has to be replaced by $ln\left(\frac{1-s}{2}\right)$.

3.2. Strong Singularities

There is also strong singularity in the integral of the left hand side of Eq. (4), which take the following form upon substitution of Eq. (2).

$$\int_L \{N\}^T \frac{-1}{2\pi} \frac{i\omega}{C_s} \frac{\partial r}{\partial n} K_1\left(\frac{i\omega r}{C_s}\right) d\, L_e \tag{12}$$

Singularity occurs in this integral when the source and observation points coincide in which case the term $\frac{\partial r}{\partial n}$ becomes zero and the function K_1 tends to infinity. As a result, their product and thus the integrand are not uniquely defined. However, It can be shown that for small values of r, the integrand would be zero and consequently the above integral vanishes for singular linear elements.

4. Determination of the Ground Response Subjected to Harmonic SH Waves

Figure (3) shows the propagation of *SH* wave into a half space. The direction of incident and reflected waves and the direction of particles motion in plane of wave front are all illustrated in this figure; θ_i and θ_r are the angle of incident and reflected waves, respectively. From the traction free condition of half space surface it can be shown that the angle and amplitude of incident and reflected waves are the same. Details of stress and displacement fields calculations in the domain can be found in reference [31].

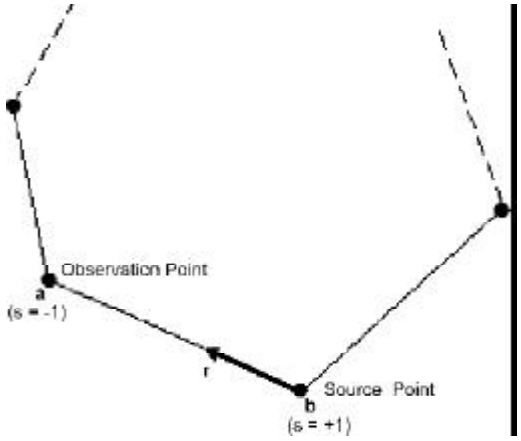

Figure 2. Position of source and observation points in case 2 singularity.

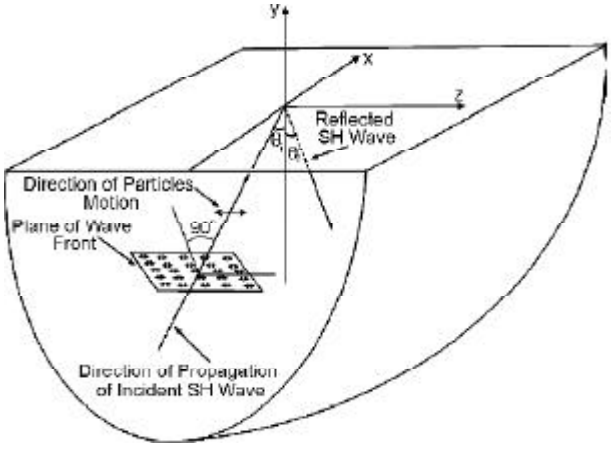

Figure 3. Propagation of SH waves in half space.

Now suppose that a canyon of irregular geometry has been cut from a half space, and that the dynamic response of this medium subjected to a two dimensional *SH* wave is under investigation. The medium is assumed to be homogeneous, viscoelastic and isotropic and the incident wave to be traveling vertically, $\theta_i = 0$, Figure (4). The total response of the medium, both displacement and traction, can be obtained by summing up two distinct responses as follows:

$$U_z = U_z^{ff} + U_z^s \tag{13}$$

$$P_z = P_z^{ff} + P_z^s \tag{14}$$

where U_z, U_z^{ff} and U_z^s are, respectively, the total, free field and scattered displacements and P_z, P_z^{ff} and P_z^s their associated tractions.

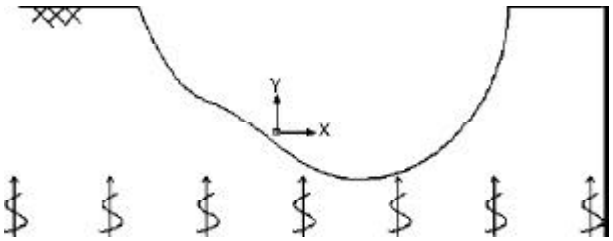

Figure 4. Canyon topography and the upcoming SH wave.

The free field displacement, U_z^{ff}, and traction, P_z^{ff}, at the hypothetical canyon surface are determined analytically from the half space solution. Since the canyon surface is traction free, Eq. (14) gives:

$$P_z^s = -P_z^{ff} \tag{15}$$

along the canyon surface, where P_z^s is the traction due to the scattered waves, and $P_z^s = 0$ elsewhere on the medium horizontal surface, see Figure (5). With the natural boundary conditions being prescribed along all domain boundaries, the displacements due to scattering of the waves are determined by using *BEM*, Eq. (6), as follows:

$$[F]\{U_z^s\} = [G]\{p_z^s\} \tag{16}$$

which when premultiplied by $[F]^{-1}$ one gets:

$$\{U_z^s\} = [F]^{-1}[G]\{p_z^s\} \tag{17}$$

The total displacement field of the medium is now calculated by summing up the displacements due to scattering and those due to free field response.

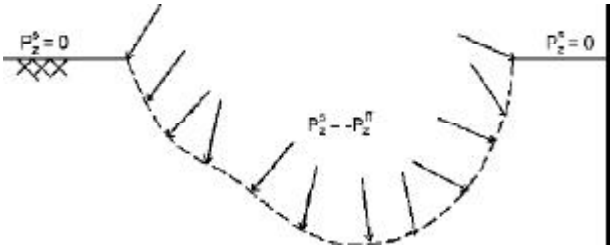

Figure 5. Natural boundary condition for the scattered field problem.

5. Application of the Technique

5.1. Introduction

Based on the procedures outlined in section 4, a computer program was developed. To limit the medium extent and minimize computational cost in the boundary element solution, enclosing elements introduced by Ahmad and Banerjee [32], were employed to represent the infinitely extending boundaries. These have been used by other researches for diffraction of *SH* waves [33], as well as *P* and *SV* waves [34].

In section 5.2 which follows, the results of the verification of the presented technique and developed code as applied to the case of a half space with single semicircular canyon will be presented. In section 5.3, further results regarding the same canyon will be studied. Finally, in section 5.4 the response of a half space with two adjacent semicircular canyons having different distances in between will be investigated.

5.2. Technique and Code Verification-Case of Single Semicircular Canyon

To test the credibility of the outlined procedure and verify the prepared code, the response of a semicircular canyon of radius *a* subjected to a vertically traveling *SH* wave, was studied and results compared to cited solutions. The plane harmonic *SH* wave, having a circular frequency ω and unit amplitude, propagates in the homogenous, viscoelastic and isotropic medium with shear wave velocity C_s. Material damping of viscoelastic medium, β, can be incorporated in the analysis by replacing shear modulus μ with its complex value [35] as:

$$\mu^* = \mu(1 + 2i\beta) \tag{18}$$

which gives, by Eq. (3), the complex shear wave velocity for viscoelastic material as:

$$C_s^* = C_s(1+i\beta) \quad (19)$$

The canyon and its surrounding and underlying medium is shown in Figure (6). In this figure, *ABCD* represents the ground surface and dashed semicircular of radius 7*a* represents the enclosing boundary; the radius was determined by trial and error to get accurate results with minimum computational effort.

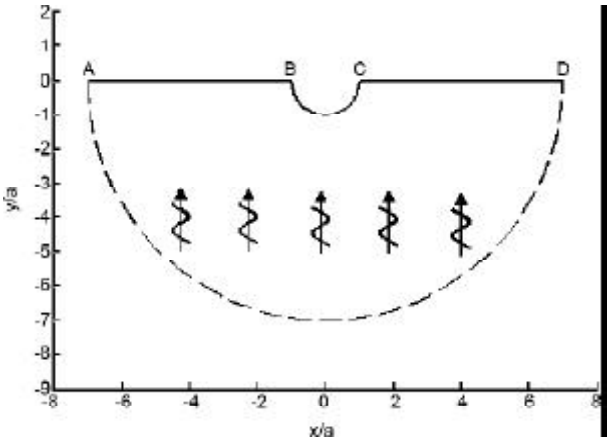

Figure 6. Semicircular canyon in a half space under vertically incident SH waves.

For boundary element analysis, the medium boundary was discretized into 248 linear elements by 252 nodes, of which 65 nodes and 64 elements are located on the enclosing boundary. In order to properly define the corners and traction discontinuities, some dummy nodes have to be introduced in the model; two nodes are defined at one point. For the case at hand, four dummy nodes are considered at points *A*, *B*, *C*, and *D* in the model. Analysis was then carried out for a 5% material damping, and the results were compared to the closed form solution of Trifunac [4]. The variation of surface displacement amplitude thus obtained by boundary element method versus the dimensionless distance x/a for the dimensionless frequency of 1 is shown in Figure (7) by dots. The dimensionless frequency is defined as:

$$\eta = \frac{\omega a}{\pi C_s} \quad (20)$$

which contains the property of the medium, C_s, the incident wave, ω, and canyon geometry, *a*. The solid line in Figure (7) corresponds to the closed form solution of Trifunac [4] obtained by using complex shear wave velocity to incorporate the material damping. Figure (7) indicates that closed

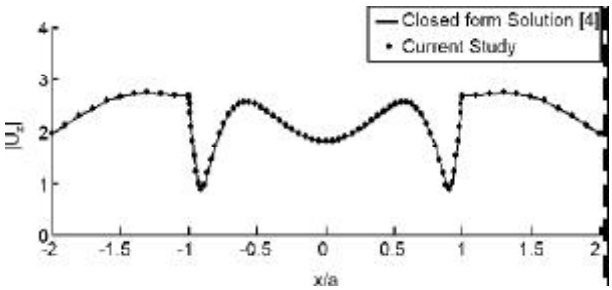

Figure 7. Distribution of displacement amplitude in and around the canyon surface.

form and numerical solutions match perfectly. With this technique and code validation, it can be applied to other cases for which no solution is, yet, at hand.

5.3. Extended Results of Single Semicircular Canyon

Surfaces with irregularities when subjected to seismic waves results in different responses along the irregular surface and the nearby ground surface as compared to the case of flat one. To determine the extent of the free surface around the canyon which is influenced by the presence of the semicircular canyon in the viscoelastic half space when subjected to *SH* waves, the amplitude of surface displacement for higher values of dimensionless distance *x/a* is shown in Figure (8). It clearly shows that the displacement amplitude decreases by increasing absolute value of *x/a* and that it fluctuates around the constant value of 2, which is the displacement amplitude of a half space surface subjected to vertically incident *SH* wave in the absence of any canyon, i.e. U_z^{ff}.

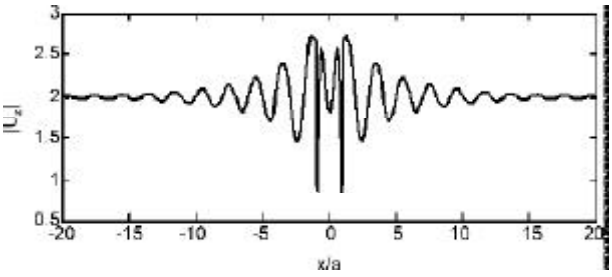

Figure 8. Distribution of displacement amplitude in and around the canyon surface for η = 1 and β = 0.05.

As $|U_z - U_z^{ff}|$ represents the amplitude of scattered wave field, its variation versus *x/a* is shown in Figure (9). This figure indicates that the amplitude of scattered waves decrease gradually with increasing

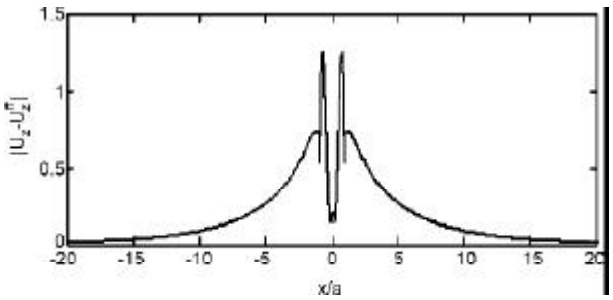

Figure 9. Distribution of scattered displacement amplitude in and around the canyon surface for $\eta = 1$ and $\beta = 0.05$.

x/a but still has a considerable value even at far away points; e.g. 0.085 at a point 9 times canyon radius farther than the canyon edge.

The variation of amplitudes of total and scattered wave displacements for points at distances *x/a* equal to 1.5, 2, 3, 5 and 10 versus dimensionless frequency η and for $\beta = 5\%$ are illustrated in Figures (10) and (11), respectively. In contrast to the amplitude of total wave responses of nearby ground surface for different *x/a*, Figure (10), which do not show a consistent variational pattern, the amplitude of scattered wave displacements, Figure (11) shows similar variational trend versus η for different *x/a*. All curves attain their absolute maximum value at $\eta = 0.45$ and the amplitude of scattered wave displacement decreases as η increases but with a decreasing rate as *x/a* gets smaller.

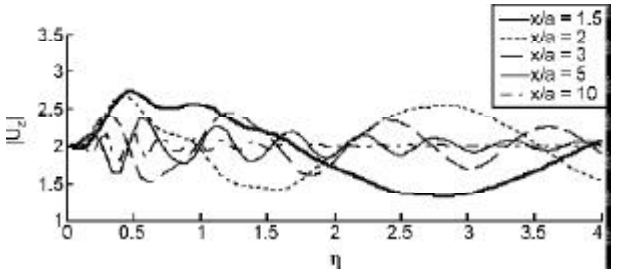

Figure 10. Variation of amplitude of total wave response of different surface points of a half space with circular canyon for different η's and $\beta = 5\%$.

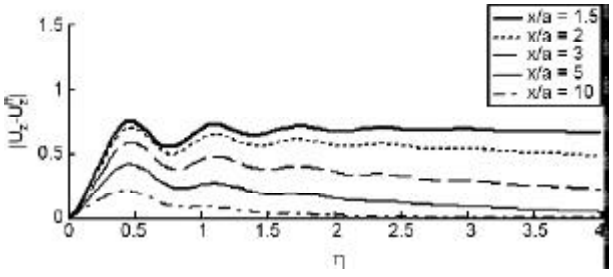

Figure 11. Variation of amplitude of scattered wave response of different surface points of a half space with circular canyon for different η's and $\beta = 5\%$.

5.4. The Case of Two Adjacent Semicircular Canyons

The boundary element method can be used to investigate the interaction of two adjacent canyons when subjected to vertically traveling plane harmonic *SH* waves. The required steps to analyze this case are similar to those for the case of a single canyon. Therefore, the tractions due to free field response along the hypothetical canyon surfaces are first computed analytically. These tractions are then reversed and exerted to the canyon surfaces to evaluate the scattered displacements using *BEM*. The total response is thus determined by summing up the free field and scattered wave responses.

The case of a homogenous, viscoelastic and isotropic half space with two semicircular canyons with radius *a*, being a distance *d* apart subjected to a vertically traveling plane harmonic *SH* waves, Figure (12), of having different dimensionless frequency, η, have been studied by the developed and validated computer code and their results will be presented hereafter. For all the cases material damping has been considered. For the case of boundary element solution, the boundary of medium contains 332 linear elements and 338 nodes, including 6 dummies, along the top surface and 64 linear enclosing elements.

The amplitude of displacement along the ground surface for dimensionless frequency of 1, when the distance of two canyons is set equal to 0.5*a*, is shown in Figure (13). The geometry of the surface irregularities are also shown in this figure. As the geometry of the model and the loading condition are symmetric, the resulted displacement is also symmetric. It is evident that the presence of canyons has resulted in a maximum deviation in surface displacement from that of a flat surface.

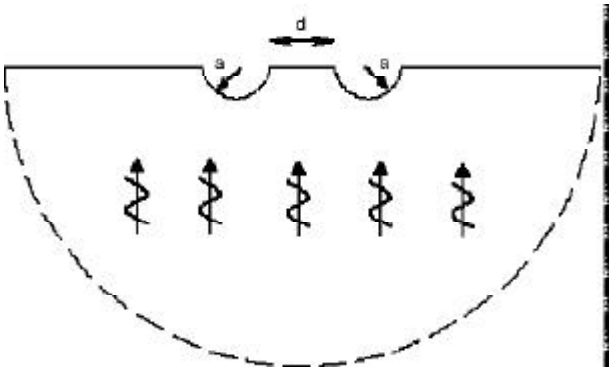

Figure 12. Double semicircular canyons in half space subjected to vertically SH waves.

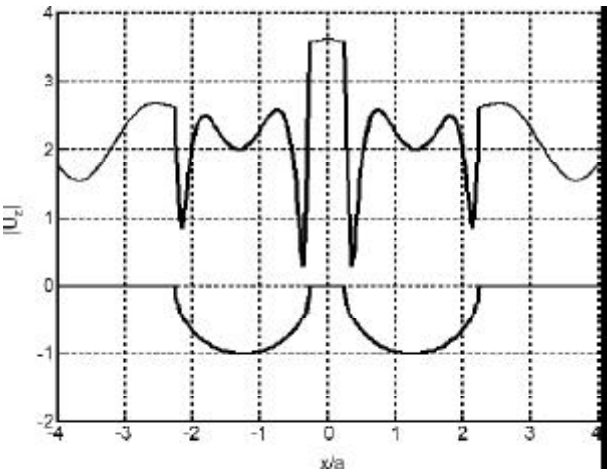

Figure 13. Displacement amplitude of ground surface for d = 0.5a, $\eta = 1$ and $\beta = 5\%$.

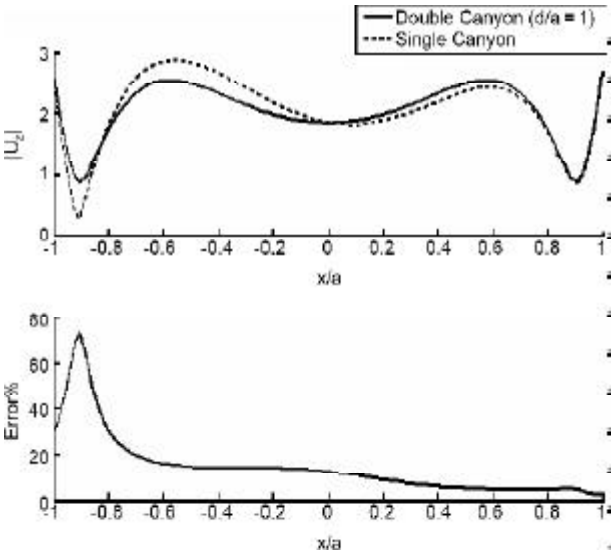

Figure 14. Displacement amplitude of single and double canyons and resulted error for d/a = 1, $\eta = 1$ and $\beta = 0.05$.

The amplitudes of difference in displacement between single and double canyons along the canyon surface would be a suitable criterion of canyons' interaction. This difference, when normalized by the displacement amplitude of the single canyon can serve as an indicator of the error of the analysis of an individual semicircular canyon without considering its interaction with the existing nearby canyon.

$$error\% = \frac{|u_d - u_s|}{|u_s|} \times 100 \qquad (21)$$

where u_s and u_d are displacements of single and double canyons, respectively. Figure (14) shows the variation of displacement amplitude response of single and double semicircular canyons versus distance for $d/a = 1$, $\eta = 1$ and $\beta = 5\%$ along with its error variation. In this figure, and for the double semicircular canyons, the right hand side canyon surface response is presented, with x' being measured from the center of right hand side semicircular canyon. The maximum error, as defined in Eq. (21) is 72.58% which occurs at x'/a equal to -0.904.

The response of each canyon of double semicircular canyons very much depends on how far it is located from the other one and also the incident wave frequency. Analyses have been made for distance of 2*a*, 4*a* and 8*a* and their results for right hand canyon are shown in Figures (15), (16) and (17), respectively for η equal to 0.45, 1 and 1.5. For comparison, the response of a single canyon is also shown in these figures.

It is clearly evident from Figures (15), (16) and (17) that the transverse displacement of double

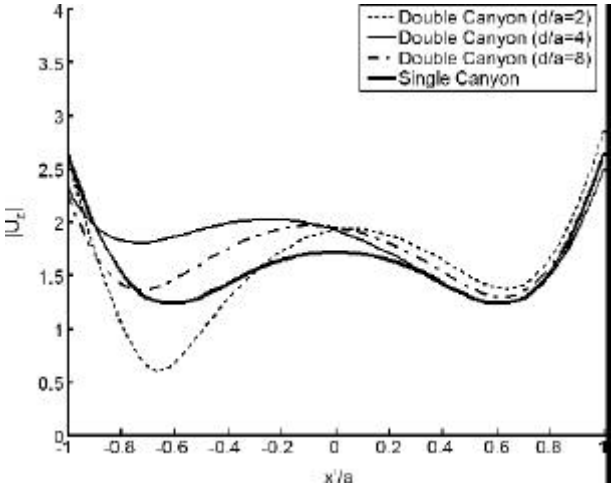

Figure 15. Displacement amplitude of the right hand canyon surface for different d/a, $\eta = 0.45$ and $\beta = 0.05$.

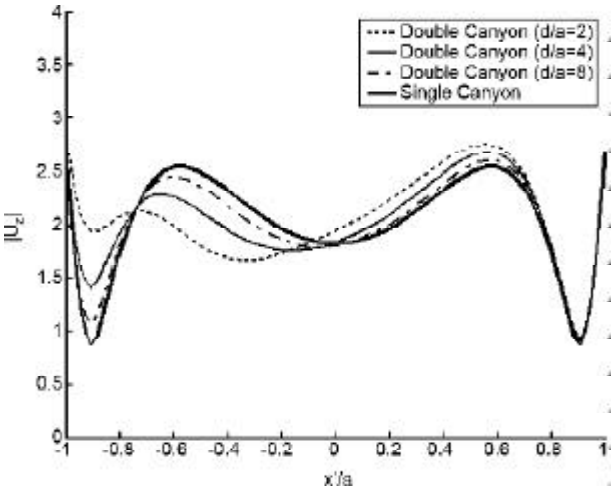

Figure 16. Displacement amplitude of the right hand canyon surface for different d/a, $\eta = 1$ and $\beta = 0.05$.

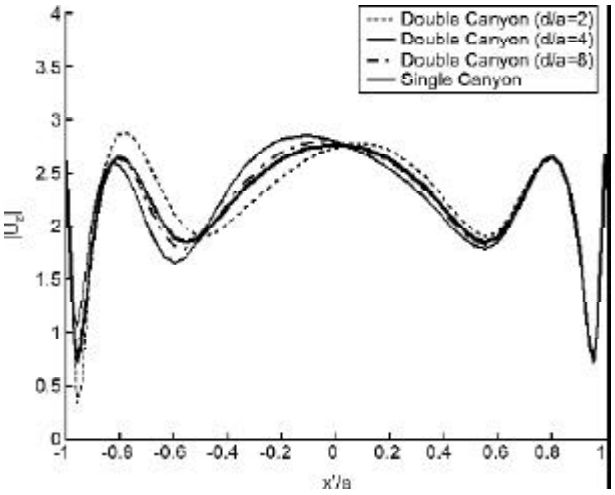

Figure 17. Displacement amplitude of the right hand canyon surface for different d/a, $\eta = 1.5$ and $\beta = 0.05$.

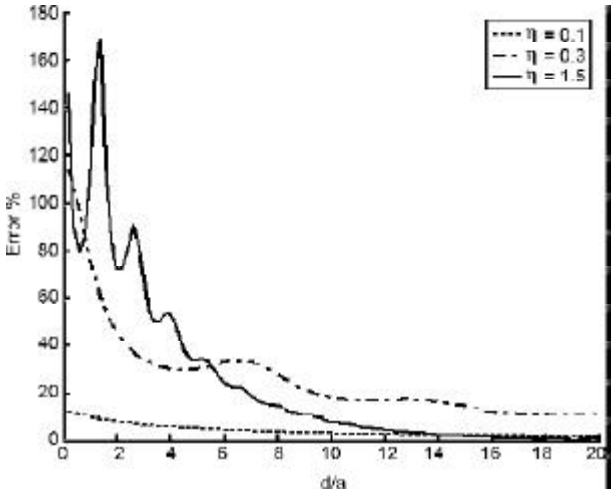

Figure 18. Error distribution versus dimensionless distance d/a, for some values of η.

canyons surface converges to that of a single one as the dimensionless distance d/a increases. To study the sensitivity of response of double canyons system with *d/a* and η, the case for different values of *d/a* and η was solved and error as defined in Eq. (21) were calculated; the maximum errors are all shown in Table (1). Variation of error percent versus *d/a* for three values of η are also shown in Figure (18).

Considering the error percent in Table (1), and the diagrams of Figure (18), the following conclusions can be drawn. In this regard a maximum error percent of 10 is considered acceptable.

1. For $\eta \leq 0.1$, the interaction of the two canyons can be discarded for all values of *d/a*.
2. For given η, the error attains its local maximum value at canyon distances corresponding to multiple of incident wave wavelength. Thus, more and more fluctuation in error percent occurs for larger η's, see Figure (18).
3. The first local maximum of error percent for each *d/a* is highlighted in Table (1). It is seen that these maxima occur in the frequency rage of $0.3 \leq \eta \leq 0.45$. This could be anticipated as it was concluded in section 5.3 that for a single canyon the maximum scattering occurs at $\eta = 0.45$ regardless of the distance where it is monitored, refer to Figure (11), and one expect to see higher interaction between two canyons where, in the frequency range, there is high scattering.
4. It is evident from Table (1) and Figure (18) that within a 10% error bound, there is no need to consider interaction of two canyons subjected to vertically incident harmonic *SH* waves having any frequency, if these are more than 20 times canyon radius apart.

Table 1. Comparison of computed maximum errors for different values of d/a and η.

?	d/a = 1	d/a = 2	d/a = 5	d/a = 10	d/a = 15	d/a = 20	d/a = 25
0.05	2.8	2.3	1.6	1.2	0.9	0.8	0.6
0.1	9.7	8.0	5.3	3.2	2.3	2.0	1.7
0.15	21.8	17.6	9.5	5.4	4.8	3.4	2.7
0.2	39.6	28.5	12.9	10.4	6.6	5.4	4.0
0.3	76.0	45.4	29.8	18.3	14.3	**10.3**	**6.8**
0.4	**83.0**	52.1	50.7	**26.7**	**15.9**	10.0	6.5
0.45	80.9	**52.2**	**50.8**	24.6	13.9	8.6	5.6
0.5	77.5	51.9	45.9	21.3	12.8	8.1	4.9
0.6	69.0	53.3	36.5	22.6	10.7	6.2	3.5
0.8	63.0	68.7	42.3	15.6	6.8	3.1	1.4
1	72.6	122.9	36.9	15.0	5.4	2.2	0.9
1.5	109.7	72.0	33.5	7.8	1.8	1	1.1
2	223.5	120.9	30.6	4.7	1.2	1.1	1.8

6. Concluding Remarks

The ability of the boundary element method in considering the effects of irregular topography on scattering of vertical plane harmonic *SH* waves was investigated. Solution was sought by combining closed form solutions of singular integrals with boundary element method. In the latter, linear elements in conjunction with dummy nodes and enclosing elements were utilized to acquire more accurate results. It was concluded that the presence of a semicircular canyon of radius *a* changes the free field motion of a half space and affects the seismic response of the ground surface even at points as far

as 10*a*. Also it was shown that the interaction of two semicircular shaped canyons would very much depend on the dimensionless frequencies. In double semicircular canyons the response of each canyon, as compared to a single one, is also highly affected by the distance between the canyons. For material damping of 5% and within a 10% error bound, the interaction of two similar semicircular canyons would be significant if the distance between the two is less than 20 times canyons' radius, and in such a case both canyons have to be modeled simultaneously in the analysis.

References

1. Sanchez-Sesma, F.J. (1990). "Elementary Solutions for Response of a Wedge-Shaped Medium to Incident SH and SV Waves", Bull. Seism. Soc. Am., **80**(3), 737-742.

2. Tsaur, D.-H. and Chang, K.-H. (2008). "An Analytical Approach for the Scattering of SH Waves by a Symmetrical V-Shaped Canyon: Shallow Case", *Geophysical Journal International*, **174**(1), 255-264.

3. Qui, F. and Liu, D. (2005). "Antiplane Response of Isosceles Triangular Hill to Incident SH Waves", *Earthquake Engineering and Engineering Vibration*, **4**(1), 37-46.

4. Trifunac, M.D. (1973). "Scattering of Plane SH Waves by a Semi-Cylindrical Canyon", *Earthquake Engineering Structural Dynamic*, **1**, 267-281.

5. Wong, H.L. and Trifunac, M.D. (1974). "Scattering of Plane SH Waves by a Semi-Elliptical Canyon", *Earthquake Engineering Structural Dynamic*, **3**, 157-167.

6. Mow, C.C. and Pao, Y.H. (1971). "Diffraction of Elastic Waves and Dynamic Stress Concentrations", Report R-482-PR, Rand Corp., Santa Monica, California.

7. Yuan, X. and Men, F.-L. (1992). "Scattering of Plane SH Waves by a Semicylindrical Hill", *Earthquake Engineering Structural Dynamic*, **21**, 1091-1098.

8. Yuan, X. and Liao, Z.-P. (1996). "Surface Motion of a Cylindrical Hill of Circular-Arc Cross-Section for Incident Plane SH Waves", *Soil Dynamic Earthquake Engineering*, **15**, 189-199.

9. Lee, V.W., Luo, H., and Liang, J. (2006). "Antiplane SH Waves Diffraction by a Semicircular Cylindrical Hill Revisited: An Improved Analytic Wave Series Solution", *Journal of Engineering Mechanics, ASCE*, **132**(10), 1106-1114.

10. Aki, K. and Larner, K.L. (1970). "Surface Motion of a Layered Medium Having an Irregular Interface due to Incident Plane SH Waves", *Jouranl Geophys. Res.*, **75**(5), 933-954.

11. Bouchon, M. (1973). "Effect of Topography on Surface Motion", Bull. Seism. Soc. Am., **63**(3), 615-632.

12. Geli, L., Bard, P.-Y., and Jullien, B. (1988). "The Effect of Topography on Earthquake Ground Motion: A Review and New Results", Bull. Seism. Soc. Am., **78**(1), 42-63.

13. Boore, D.M. (1972). "A Note on the Effect of Simple Topography on Seismic SH Waves", Bull. Seism. Soc. Am., **62**, 275-284.

14. Bettess, P. (1977). "Infinite Elements", *International Jouranl for Numerical Methods in Engineering*, **11**(1), 53-64.

15. Lysmer, J. and Kuhlemeyer, R. (1969). "Finite Dynamic Model for Infinite Media", *Journal of Engineering Mechanics Division, ASCE*, **95**(4), 859-877.

16. Zhang, C. and Zhao, C. (1988). "Effect of Canyon Topography and Geological Conditions on Strong Ground Motion", *Earthquake Eng. Struct. Dyn.*, **16**, 81-97.

17. Liu, J. and Lu, Y. (1998). "A Direct Method for Analysis of Dynamic Soil-Structure Interaction Based on Interface Idea", *Dynamic Soil-Structure Interaction*, Current Research in China and Switzerland, Edited by Chuhan, Z. and Wolf, J.P., 261-276.

18. Sanchez-Sesma, F.J. and Rosenblueth, E. (1979).

"Ground Motion at Canyons of Arbitrary Shape under Incident SH Waves", *Earthquake Engineering Structural Dynamic*, **7**, 441-450.

19. Zhang, L. and Chopra, A.K. (1991). "Three-Dimensional Analysis of Motions around a Uniform Canyon in a Homogeneous Half-Space", *Earthquake Engineering Structural Dynamic*, **20**, 911-926.

20. Eshraghi, H. and Dravinski, M. (1989). "Scattering of Plane Harmonic SH, SV, P and Rayleigh Waves by Non-Axisymmetric Three Dimensional Canyons: A Wave Function Expansion Approach", *Earthquake Engineering Structural Dynamic*, **18**(7), 983-998.

21. Kamalian, M., Gatmiri, B., Sohrabi-Bidar, A., and Khalaj, A. (2007). "Amplification Pattern of 2D Semi-Sine Shaped Valleys Subjected to Vertically Propagating Incident Waves", Communications in Numerical Methods in Engineering, **23**, 871-887.

22. Rahimian, M., Omidvar, B., Derakhshan, H., and Noorzad, A. (2007). "Effects of Arbitrary Shaped Surface Topographies on Earthquake Ground Motion Using Boundary Element Method in Time Domain", *Iranian Journal of Science and Technology*, **31**(B5), 473-485.

23. Kawase, H. (1988). "Time-Domain Response of a Semi-Circular Canyon for Incident SV, P, and Rayleigh Waves Calculated by the Discrete Wave Number Boundary Element Method", Bull. Seism. Soc. Am., **78**(4), 1415-1437.

24. Kim, J. and Papageorgiou, A.S. (1993). "Discrete Wave-Number Boundary-Element Method for 3-D Scattering Problems", *Journal of Engineering Mechanics, ASCE*, **119**(3), 603-624.

25. Bard, P.-Y. and Tucker, B.E. (1985). "Underground and Ridge Site Effects: A Comparison of Observation and Theory", Bull. Seism. Soc. Am., **75**, 905-922.

26. Sanchez-Sesma, F.J. and Campillo, M. (1993). "Topographic Effects for Incident P, SV, and Rayleigh Waves", *Tectonophysics*, **218**, 113-125.

27. Ding, G. and Dravinski, M. (1996). "Scattering of SH Waves in Multilayered Media with Irregular Interfaces", *Earthquake Engineering Structural Dynamic*, **25**, 1391-1404.

28. Dominguez, J. (1993). "Boundary Elements in Dynamics", Computational Mechanics Publications, Southampton and Boston.

29. Ameen, M. (2001). "Boundary Element Analysis; Theory and Programming", Alpha Science International, UK.

30. Banerjee, P.K., Wang, H.C., and Ahmad, S. (1992). "Multi-Region Periodic Dynamic Analysis by BEM of 2-D, 3-D and Axisymmetric Problems", Chapter 2 in Advanced Dynamic Analysis, Development in Boundary Methods, **7**, Elsevier Appl. Scie., London, 27-74.

31. Achenbach, J.D. (1975). "Wave Propagation in Elastic Solids", North-Holland Publishing Co. Amsterdam (Elsevier).

32. Ahmad, S. and Banerjee, P.K. (1988). "Multi-Domain BEM for Two-Dimensional Problems of Elastodynamics", *International Journal for Numerical Methods in Engineering*, **26**(4), 891-911.

33. Heymsfield, E. (1997). "Infinite Domain Correction for Anti-Plane Shear Waves in a Two-Dimensional Boundary Element Analysis", *International Journal for Numerical Methods in Engineering*, **40**(5), 953-964.

34. Kamalian, M., Gatmiri, B., and Sohrabi-Bidar, A. (2003). "On Time-Domain Two-Dimensional Site Response Analysis of Topographic Structures by BEM", *Journal of Seismology and Earthquake Engineering (JSEE)*, **5**(2), 35-45.

35. Kausel, E. and Roesset, J. (1974). "Dynamic Stiffness of Circular Foundation", *Journal of Engineering Mechanics Division, ASCE*, **101**(6), 771-785.